High Impedance Fault Identification on Distribution Networks

W. C. Santos, *Student Member, IEEE*, F. V. Lopes, *Member, IEEE*, N. S. D. Brito, *Member, IEEE*, B. A. Souza, *Senior Member, IEEE*

***Abstract*-- This paper presents a transient-based algorithm for high impedance fault identification on distribution networks. It uses the discrete wavelet transform to monitor high- and low-frequency voltage components at several points of the power system, being able to indicate the most likely area within which the disturbance has occurred, without requiring data synchronization nor the knowledge of feeder or load parameters. The proposed algorithm is evaluated through electromagnetic transients program simulations of high impedance faults in a 13.8 kV system modeled from actual Brazilian distribution grid data. Solid faults, capacitor bank switching and feeder energization are also simulated, considering the system with and without distributed generation. Obtained results show that the algorithm significantly reduces the search field of the high impedance fault, reliably distinguishing it from other disturbances.**

***Index Terms*—Power distribution protection, electromagnetic transient analysis, fault diagnosis, fault location, high impedance faults, power systems, wavelet transforms.**

I. Introduction

ELECTRIC transmission and distribution utilities have been increasingly asked to minimize power outage times and operating costs due to short-circuits. In this context, the development of fast and reliable techniques able to diagnose faults in both transmission and distribution grids is an issue that has been widely studied worldwide for decades.

In distribution networks (DN), a special class of faults called high impedance faults (HIF) is difficult to deal with, since it is usually not detected by conventional overcurrent-based protection devices [1], [2]. In fact, HIF current levels are normally similar to those observed during the steady-state, what jeopardizes the operation of conventional protection and fault location devices. As a consequence, the population may be exposed to the risk of electric shock and the system recovery is delayed.

The Brazilian Association of Electricity Distributors (Abradee) annually discloses the number of accidents in the Brazilian electrical distribution network. From 2001 to 2014, the number of reported accidents in the DN has decreased from 1046 to 777 [3]. In the same period, the number of deaths has also been reduced from 381 to 299 [3]. However, even with the reduction of accidents over the recent years, HIFs have been repeatedly referred to as one of the major causes of deaths. For instance, in 2013 and 2014, HIFs were the third major cause of accidents, resulting in 30 and 53 deaths, respectively. These numbers highlight the need for more reliable solutions to identify and locate HIFs on distribution grids.

In the literature, several methods used for fault detection and location in transmission lines are available [4]–[6]. There are also several papers which report HIF detection techniques [7]-[13]. Nevertheless, the HIF identification accompanied with its location estimation is still a challenge. In fact, due to DN topology and observability issues, traditional transmission line fault location methods do not suit for this type of system [14],[15]. Even using more sophisticated algorithms, such as those based on the theory of traveling waves, the fault location procedure is still a problem. Since the distribution feeders are usually short, the conductors' travel time is very small, so that extremely high sampling rates would be required [15].

With the advent of digital technology and communication networks, the number of monitoring points along the power systems has increased, boosting several developments toward finding new solutions to diagnose HIFs. Furthermore, the real-time monitoring of DNs has gained importance over the years, motivating the development of techniques able to combine effectiveness, velocity and simplicity [15], [16]. In this context, fault-induced transient-based approaches have been reported [17]–[21].

In this work, an algorithm for HIF identification on DNs is proposed. It detects the HIF, distinguishes it from other disturbances, and estimates the most likely area of the system within which the disturbance has occurred, reducing the search field of the fault. The technique analyzes the HIF-induced low- and high-frequency voltage components at strategic points of the DN, requiring neither data synchronization nor parameters of feeders or loads. To do so, energy spectrums of detail- and approximation-wavelet coefficients are computed at the monitored buses and used to identify the area where the HIF is located. The proposed algorithm is evaluated through Electromagnetic Transients Program (EMTP) simulations of HIFs in a 13.8 kV DN. For this purpose, a HIF model based on two series time-varying resistances controlled by the Transient Analysis of Control Systems (TACS) [22] was modeled. The obtained results show the proposed approach is able to detect the HIF, to distinguish it from solid faults and switching maneuvers, and to reduce the disturbance search field, speeding up the HIF identification.

This work was supported by the Brazilian Coordination for Improvement of Higher Education Personnel (CAPES).

W. C. Santos, N. Brito and B. Souza are with the Department of Electrical Engineering, Federal University of Campina Grande (UFCG) (e-mails: wellinsilvio.santos@ee.ufcg.edu.br, {nubia,benemar}@dee.ufcg.edu.br).

F. V. Lopes is with the Department of Electrical Engineering, University of Brasília (UnB) (e-mail: felipevlopes@unb.br).

II. High Impedance Fault Features

HIFs occur when an energized conductor of the primary network makes an electrical contact with a surface of high resistive value, resulting in overcurrent levels that are not enough to sensitize the conventional protection systems. Consequently, the fault is not cleared, exposing the population to the risk of electric shock and compromising the integrity of system and costumer equipment. Usually, the distribution utilities detect and locate HIFs based on costumers' complaints, which are sorted out in call-centers and, then, informed to the operation center and maintenance crews.

According to [23], HIFs generally cause the appearance of electric arcs, so that fault currents typically have the following characteristics:

- *Asymmetry*: Fault current has different peak values for positive and negative half cycle;
- *Nonlinearity:* Voltage-current characteristic curve is nonlinear;
- *Buildup:* Current magnitude increases to its maximum value gradually;
- *Shoulder:* Buildup stops for few cycles;
- *Intermittence:* Some cycles in which the energized wire interrupts the contact with the soil.

Fig. 1 shows an example of a HIF field test record. Nonlinearities and asymmetries occur in the whole signal, whereas both buildup and shoulder show up around 0.55 s and the intermittence at around 0.3 s. HIFs also generate electromagnetic transients between 2 and 10 kHz, mainly due to the intermittent permanence of the wire on the soil [24]. These high frequency components may be extracted through suitable signal processing techniques and then used to identify HIFs in addition to conventional overcurrent relays, guaranteeing more reliable fault detections.

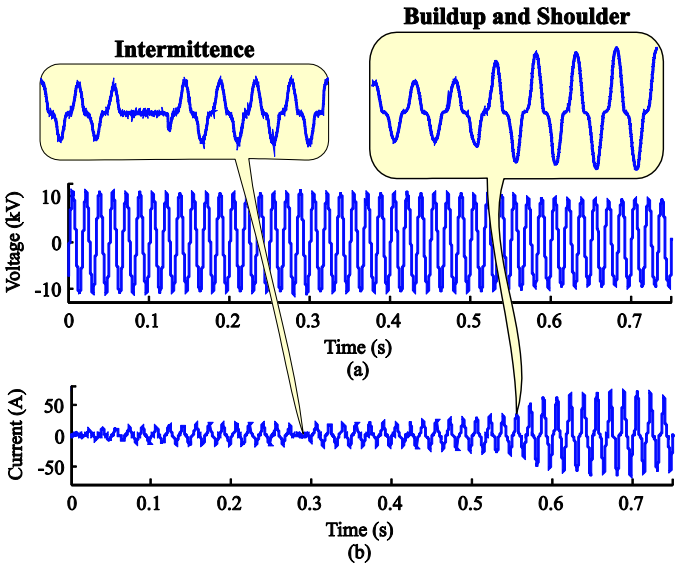

Fig. 1. Actual HIF oscillographic record: (a) Voltage; (b) Current.

III. Proposed HIF Identification Method

The proposed algorithm is based on the analysis of HIF-induced high- and low-frequency components, which are extracted from the monitored signals using the discrete wavelet transform (DWT) [25]. The main idea is to associate the HIF closeness with each monitored point by the analysis of the measured fault-induced transients at different buses of the system. By doing so, the search field of the fault can be reduced, speeding up the HIF identification process.

Other sources of electromagnetic transients in DNs can be confused with those induced by HIFs, such as solid faults and switching maneuvers of feeders and capacitor banks. Therefore, to distinguish HIFs from other events, two additional assumptions are taken into account during the proposed HIF identification procedure. The first one regards to the period during which the energy spectrum of detail-wavelet coefficients remains above a given threshold. In fact, as reported in [7], since the HIF is not detected by the protection system, its effects remain for a long period, lasting more than the maximum fault clearance time allowed by the distribution grid rules. The second assumption deals with the calculation of the energy spectrum of approximation-wavelet coefficients of voltages, which allows the detection of sags and swells. Since HIFs do not cause relevant variations in voltage signals, it can be concluded that the disturbance is not a HIF if relevant sags and swells are detected.

A. The Discrete Wavelet Transform

The discrete wavelet transform is a powerful time-frequency signal-processing tool that allows the analysis of sampled signals with localized transients [25]. For decades, such transform has been widely applied to power system problems in the area of transient analysis [15].

The DWT divides the frequency-band of the input signal into low- and high-frequency components, which are called here approximation (*c*) and detail (*d*) coefficients, respectively. These components are obtained by low- and high-pass filters (*h(k)* and *g(k)*, respectively) in cascade with down-samplers with the grade of 2 (↓2).

Fig. 2 illustrates the structure of a two-level DWT algorithm applied to an input signal *s(k)* sampled at a rate of f_s Hz[1]. Coefficients of both *h(k)* and *g(k)* filters depend on the selected mother wavelet. In this work, the Daubechies 4 (db4) is used, since it is suitable for detection of fast transients such as those induced by HIF [7], [24].

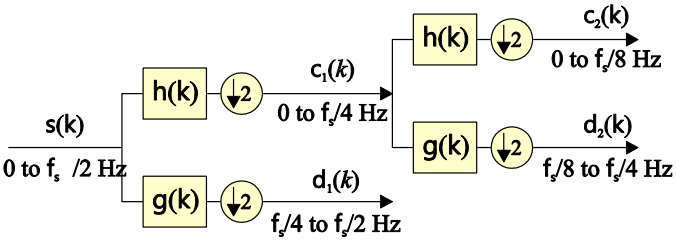

Fig. 2. Structure of two-level DWT algorithm.

[1] According to the Nyquist theorem, for an analog signal sampled at f_s Hz, the maximum frequency represented in the digitized waveform is of f_s/2 Hz.

B. Energy Spectrum of Detail and Approximation Coefficients

Several fault diagnosis techniques use the detail coefficients to detect high frequency components that show up in the monitored signals soon after the fault inception. However, electrical noises may pose difficulties for such methods, especially in the HIF cases, for which voltage and current induced transients are quite attenuated [16]. To overcome this problem, the energy spectrum of detail coefficients d — called here ξ_d — is normally used [7].

Other disturbances such as solid faults, switching maneuvers of branches and capacitor banks can cause transients enough to affect ξ_d. Thus, as HIFs do not cause significant magnitude variations in currents and voltages, the energies of the approximation coefficients c — called here ξ_c – are also calculated in the proposed algorithm. The energy ξ at a given scale j may be computed as follows:

$$\xi_d(k) = \sum_{n=k}^{k+(\Delta k_{cycle}/2j)} d_j^2(n), \quad (1)$$

$$\xi_c(k) = \sum_{n=k}^{k+(\Delta k_{cycle}/2j)} c_j^2(n), \quad (2)$$

where Δk_{cycle} is the number of samples per fundamental cycle.

In order to reduce the algorithm computational burden, only detail and approximation coefficients at the first scale (j = 1) are analyzed in the proposed approach, i.e., ξ_d and ξ_c are computed using only d_1 and c_1, respectively. Fig. 3 depicts an example of a HIF detection field test case using voltage and current ξ_d and ξ_c energies. The simulation parameters were taken from an actual Brazilian 13.8 kV DN.

One can see that the HIF beginning time is unclear in voltage and current time-domain records, but ξ_d energies present fast-risings that permit the detection of the moment at which fault-induced transients begin at the monitored terminal. Fig. 3 still shows that voltage and current ξ_c energies do not vary significantly during the HIF. On the other hand, ξ_d of voltage signals assumes higher values than those in ξ_d of current signals after the disturbance inception, so that the proposed algorithm analyzes only voltage waveform samples.

C. HIF Detection

The HIF detection algorithm is based on the identification of fast-rising energies in ξ_d waveforms and on the analysis of the period during which the transient energy remains above a self-adaptive threshold. Besides, the HIF detection also depends on the analysis of ξ_c, as mentioned before. Therefore, if ξ_d indicates the presence of transients during a period higher than the fault clearance time allowed by the system rules and ξ_c does not indicate the occurrence of sags or swells, the HIF is detected. By doing so, the proposed algorithm distinguishes solid faults and switching maneuvers from HIFs.

In some cases, such as in the presence of noises, oscillations in ξ_d may show up even during the steady-state. Similarly, low-frequency components can also present slight oscillations during the steady-state. To properly detect HIF-induced transients and correctly identify relevant voltage sags or swells, a hard thresholding procedure is applied to ξ_d and ξ_c.

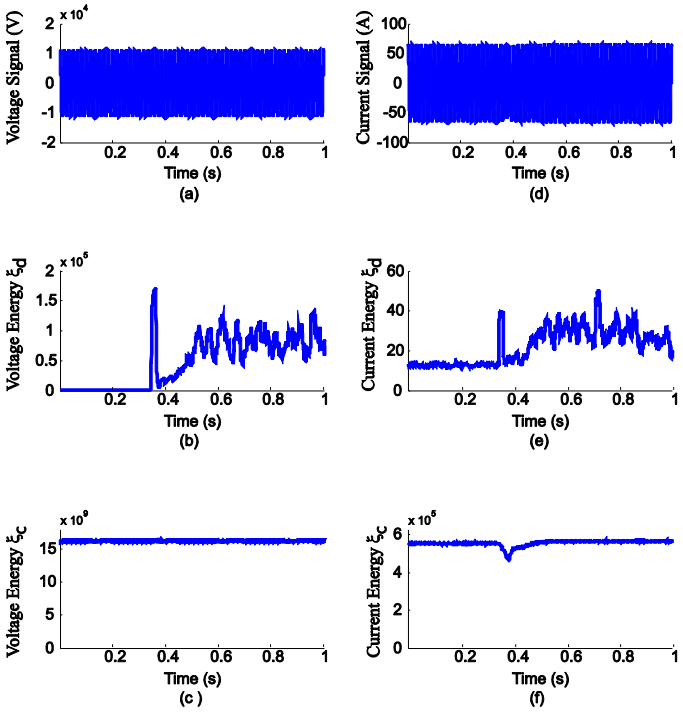

Fig. 3. Example of HIF fault detection: (a) time-domain voltage record; (b) energy of detail wavelet coefficients of voltage; (c) energy of approximation wavelet coefficients of voltage; (d) time-domain current record; (e) energy of detail wavelet coefficients of current; (f) energy of approximation wavelet coefficients of current.

The hard thresholding filtering process was originally proposed in [26] for transient detection applications using the DWT. Basically, the detail coefficients with values smaller than a given threshold are discarded and, otherwise, a transient is detected. In [26], the threshold is computed based on the maximum value of the analyzed detail coefficients verified in the whole disturbance record, what is feasible only for off-line applications. Therefore, in this work, aiming at real-time applications, instead of using the maximum signal sample value verified in the whole record, two self-adaptive thresholds ρ_d and ρ_c are adjusted at each sampling instant based on the ξ_d and ξ_c steady-state energies:

$$\rho_d = (1+\eta)\cdot \max(\xi_{d,past}), \quad (3)$$

$$\rho_c = (1-\eta)\cdot \max(\xi_{c,past}), \quad (4)$$

where $\xi_{d,past}$ and $\xi_{c,past}$ are respectively the set of ξ_d and ξ_c samples in the power frequency cycle that precedes the monitored sample, max() is a function to compute the global maximum value among the analyzed energy samples and η is a secure margin applied over the adaptive thresholds ρ_d and ρ_c. Here, η=0.1 is used, as suggested in [26]. The same secure margin is used to analyze the ξ_c energy.

Fig. 4 shows a transient detection example considering the voltage energy ξ_d. The HIF detection flag changes its logic level for '1' soon after the disturbance inception, stopping the calculation of the thresholds ρ_d and ρ_c, and triggering the HIF location algorithm, which will be described in the next section. Since the HIF is not extinguished, ξ_d presents values above ρ_d for several cycles.

According to the Brazilian power grid rules, in transmission and distribution networks with rated voltage until 345 kV, protection devices must be properly coordinated to detect and clear disturbances in a time up to 150 ms [27], [28]. Thus, if $\xi_c > \rho_c$ and $\xi_d > \rho_d$ for consecutive 150 ms after the transient detection and fuses, reclosers, and circuit breakers remain closed, the disturbance is classified as HIF. If there is a failure in the protection system and a solid fault persists in the DN for more than 150 ms, ξ_c detects voltage sags, i.e., $\xi_c < \rho_c$, ruling out the possibility of a HIF occurrence.

D. HIF Location

The exact HIF location is still a challenge for the scientific community. Most techniques proposed so far in the literature have required the knowledge of feeder data and have been applied off-line in order to use more sophisticated routines [15], limiting their use in real-time applications.

In this work, although the exact fault point is not computed, a great reduction of the search field of the HIF is achieved by the analysis of the maximum ξ_d values at different DN buses. Basically, the maximum ξ_d values at the monitored buses during the first power cycle after the first transient detection are recorded and compared to each other, assuming that the HIF is at some feeder section within the area between the three buses with the most relevant ξ_d values.

The analysis of transient magnitudes at different points of the DN can provide information regarding the area in which the fault has occurred. For instance, if a HIF is closer to Bus R than to Bus S, the transients tend to be more attenuated at Bus S [29]. Consequently, though it is impossible to estimate the exact fault point using this information, a great reduction of the search field of the HIF can be achieved. In this context, the higher the number of monitored points, the higher the reduction of the search field of the HIF, which is suitable for DNs with several monitored points and communication links available. The proposed HIF identification algorithm is summarized in Fig. 5.

IV. Simulations and Models

In order to evaluate the proposed algorithm, HIF simulations in a 13.8 kV DN were performed using the Alternative Transients Program (ATP). Besides HIFs, solid faults, switching maneuvers, simultaneous solid faults and simultaneous HIFs, considering different number and position of the monitoring devices were also simulated. Furthermore, as the proposed algorithm depends on the detection of HIF-induced transients, different sampling rates were analyzed.

A. Simulated Feeder

Fig. 6 depicts the 13.8 kV test DN simulated in ATP. It was modeled using actual data provided by a Brazilian distribution utility. In order to facilitate the DN modeling, all branches were assumed to be composed by 4 AWG wires, the feeder was modeled by using a constant distributed parameter line model, a constant impedance load model was used considering a power factor of 0.955, and loads close to each other were put together, resulting in a feeder with 90 buses.

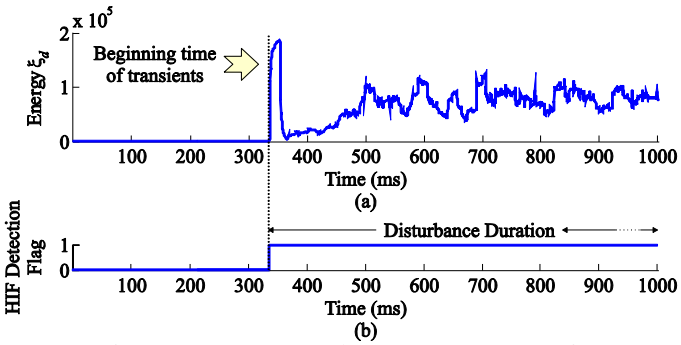

Fig. 4. HIF fault detection: (a) Energy ξ_d; (b) Transient detection flag.

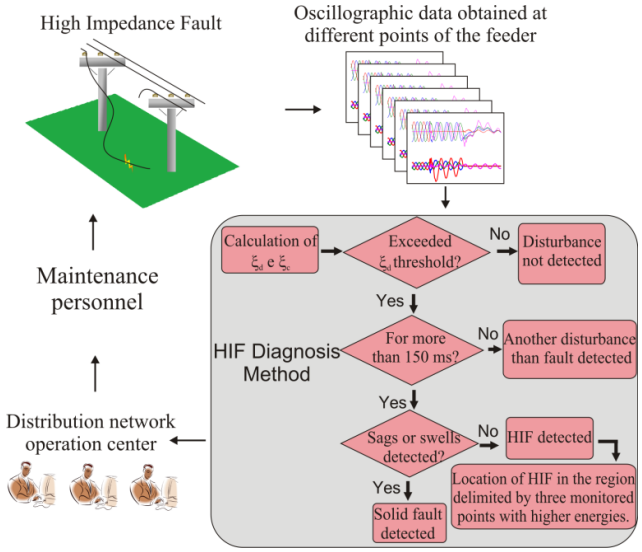

Fig. 5. Proposed HIF identification algorithm.

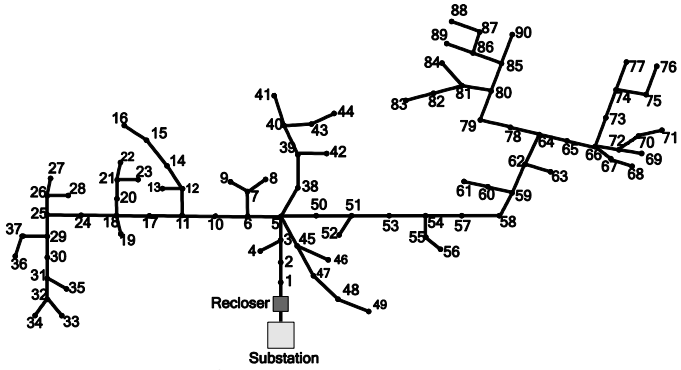

Fig. 6. Modeled 90 bus feeder.

B. Noise Simulation

Voltages and currents taken from actual oscillographic records are not purely sinusoidal, but consist of noise and harmonic components summed to a fundamental component. Since the detail coefficients *d* are sensitive to high frequency components, the noise effect on the proposed method is also taken into account. As reported in [5], the noise in power systems measurements has a normal probability distribution and is present in the whole recorded signals, irrespectively if the record is with or without disturbances. These noises are quantified by the formula of signal-to-noise ratio (SNR) [30]:

$$SNR_{dB} = 20 \cdot \log_{10}\left(A_{signal}/A_{noise}\right), \quad (4)$$

where *A* is the root mean square of the signal. In this work, the influence of a 60 dB SNR is considered.

C. The HIF Model

Fig. 7 illustrates the HIF model used in this work. The HIF model was proposed in [2] and is able to represent the set of characteristics previously illustrated in Fig. 1: nonlinearity, asymmetry, buildup, shoulder, and intermittence.

The model is composed by:

- Two time-varying resistances (TVRs), in series, and controlled by TACS [17]:
  - Resistance R1: simulates the characteristics of nonlinearity and asymmetry (providing the same characteristics at every cycle of the signal).
  - Resistance R2: simulates the phenomena of buildup and shoulder (just influencing at the beginning of the signal).
- Two time-controlled switches:
  - Switch 1: connects the resistances to the fault point and simulates the fault inception time.
  - Switch 2: connected downstream from the fault point, simulating the conductor breakage.

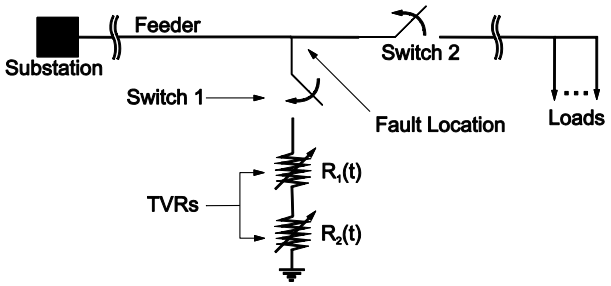

Fig. 7. HIF model.

D. Monitored Areas

In the proposed algorithm, the search field of the HIF is defined based on the number and position of the monitoring devices installed in the DN. Basically, the feeder is divided into different monitored areas, which contain one monitoring device each. If one of the three major transient energies is detected by a given device installed in a given area 'A', the feeder section within the area 'A' is selected for inspection. To better analyze the proposed algorithm performance with respect to the number and position of monitoring devices, three different scenarios were taken into account, which are detailed in Table I.

For each evaluated case, the search field reduction is considered as the relation between the number of buses that belong to the monitored areas selected for inspection and the total amount of buses in the modeled DN, i.e., 90 buses. For instance, a reduction of 50% means that 45 buses should be inspected rather than the 90 buses of the system.

E. Feeder Energization and Capacitor Bank Switching

To simulate the feeder energization case, switches between buses 10-11 and 30-31 were inserted in the modeled DN. By closing these switches, the influence of feeder energization procedures on the proposed algorithm are analyzed.

TABLE I
NUMBER/POSITION OF THE MONITORING DEVICES AND MONITORED AREAS

Scenario	Number of Monitoring Devices	Position of Monitoring Devices (at buses)	Monitored area per monitoring device
1	6	32	Bus 1 to 37
		44	Bus 38 to 44
		49	Bus 45 to 49
		54	Bus 50 to 64
		76	Bus 65 to 76
		90	Bus 78 to 90
2	6	18	Bus 1 to 37
		39	Bus 38 to 44
		47	Bus 45 to 49
		59	Bus 50 to 64
		71	Bus 65 to 76
		83	Bus 78 to 90
3	8	16	Bus 1 to 23
		32	Bus 24 to 37
		44	Bus 38 to 44
		49	Bus 45 to 49
		54	Bus 50 to 63
		64	Bus 64 to 69 and 78 to 84
		76	Bus 70 to 77
		90	Bus 85 to 90

The switching maneuver with capacitors was simulated considering capacitor banks of 1.8 Mvar and 0.9 Mvar, whose data were taken from an actual Brazilian distribution network. Here, it is assumed that the capacitor banks are both installed at the substation (see Fig. 6). Since a capacitor has intrinsic inductances and resistances besides its own capacitance [31], the lumped element model illustrated in Fig. 8 was used. It is connected in Y-isolated with the neutral connected to the ground through a capacitance C_T of 250 pF. The capacitance C represents the capacitor bank and its value in Farads is obtained from the nominal reactive power of the bank. The inductance L represents the equivalent inductance obtained from the intrinsic internal inductance of the capacitor bank and the inductance of the current limiting reactor, whose values in Henry are 5 μH and 100 μH, respectively. Finally, R_{ESR} is the equivalent series resistance of the capacitor bank. This parameter allows the simulation of losses in the capacitor bank and is represented by a single resistor in the equivalent circuit shown in Fig. 8 [31]. Here, $R_{ESR} \approx 0.001\ \Omega$ was used.

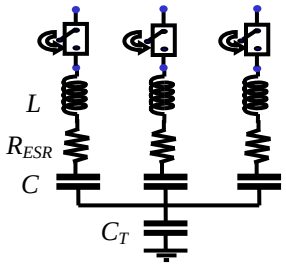

Fig. 8. Capacitor bank model.

V. Proposed Algorithm Evaluation

The proposed HIF identification algorithm evaluation is divided into six parts: 1) the sampling rate influence; 2) HIF identification considering different monitored points; 3) HIF identification considering different amounts of monitoring devices in systems with and without distributed generation; 4) HIFs at different locations; 5) Algorithm performance during solid faults, feeder branch energizations and capacitor bank switching; and 6) Simultaneous HIFs and solid faults.

A. Sampling Rate Influence

Sampling rates used during the analog-to-digital conversion of voltage and current signals have a strong influence on transient based fault diagnosis techniques. In fact, the greater the number of samples per cycle, the more accurate the representation of high frequency components. To evaluate the sampling rate influence on the proposed HIF identification algorithm, a HIF at bus 10 was simulated and the respective records at the monitored buses were analyzed using sampling frequencies of 15.36 kHz, 61.44 kHz and 107.52 kHz. In these test cases, the monitoring devices were assumed to be distributed in the DN as in the scenario 1 described in Table I. The obtained results are shown in Figs. 9, 10 and 11.

For signals sampled at 107.52 kHz, a more relevant influence of noises on the steady-state quantities is observed. Such an influence was smaller for sampling rates of 15.36 kHz and 61.44 kHz. However, for all sampling frequencies analyzed, the proposed algorithm properly detected the HIF, identifying it within the region in between buses 32, 44 and 49, resulting in a search field reduction of about 47.8%. Therefore, since the results were satisfactory for all evaluated sampling rates and considering the commercial availability of devices with f_s=15.36 kHz, only the sampling rate of 15.36 kHz will be used in the next sections of this work.

B. Using Different Monitored Points

To analyze the use of different monitored points, the proposed algorithm was applied for HIFs at buses 19, 63, 66 and 79, considering monitoring devices as in the scenarios 1 and 2 described in Table I.

Buses with the most relevant ξ_d values and the search field reduction for each evaluated case are presented in Table II. From the obtained results, it is concluded that the use of different monitored points may change the buses with the maximum ξ_d levels, but it does not compromise the algorithm performance. In fact, for both evaluated scenarios, the same search field reduction was obtained.

TABLE II
Evaluation of Different Scenarios with 6 Monitoring Points

Fault Location	Buses with Maximum ξ_d Levels		Search Field Reduction	
	Scenario 1	Scenario 2	Scenario 1	Scenario 2
19	32, 49, 44	18, 39, 47	45.56%	45.56%
63	76, 54, 49	59, 47, 83	63.33%	63.33%
66	76, 90, 54	71, 83, 59	54.44%	54.44%
79	76, 90, 54	83, 59, 71	54.44%	54.44%

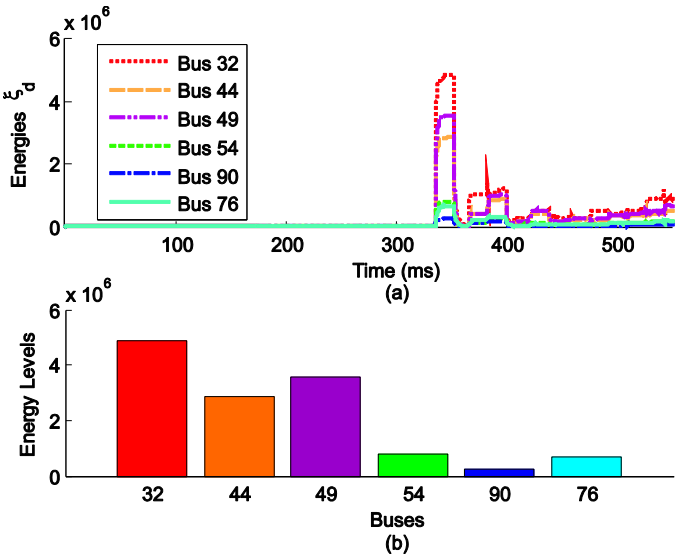

Fig. 9. Analysis of a HIF at bus 10 using a sampling rate of 15.36 kHz: (a) energies of detail coefficient of voltages; (b) maximum energy levels.

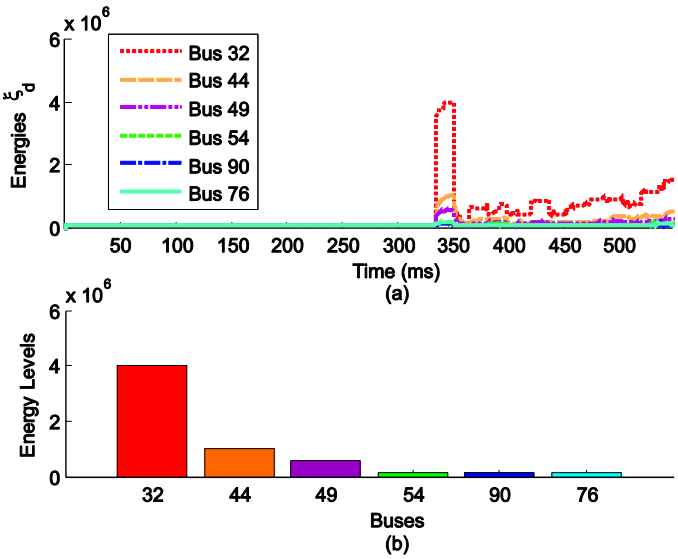

Fig. 10. Analysis of a HIF at bus 10 using a sampling rate of 61.44 kHz: (a) energies of detail coefficient of voltages; (b) maximum energy levels.

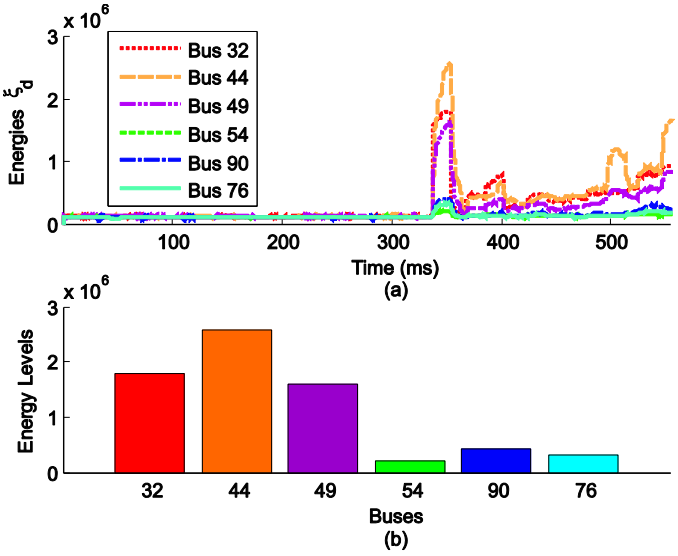

Fig. 11. Analysis of a HIF at bus 10 using a sampling rate of 107.52 kHz: (a) energies of detail coefficient of voltages; (b) maximum energy levels.

C. Using Different Amounts of Monitoring Devices in Systems With and Without Distributed Generation

The search field reduction depends directly on the number of monitoring devices in the DN. To evaluate the proposed algorithm performance when different amounts of monitoring devices are used, HIFs at buses 19, 63, 66 and 79 were simulated and, then, analyzed considering the scenarios 1 and 3 described in Table I. Since the distributed generation (DG) is a future trend of distribution networks, simulations were carried out considering the modeled system with and without DG. In cases of the system with DG, generation plants with voltage $1\angle 0^{o}$ p.u. at buses 36 and 88 were included. For the performed analysis, it was considered a wind distributed generation with penetration level of 40%. The obtained results are depicted in Tables III and IV.

TABLE III
EVALUATION WITH AND WITHOUT DG WITH 6 MONITORING POINTS

Fault Location	Buses with Maximum ξ_d Levels		Search Field Reduction	
	Without DG	With DG	Without DG	With DG
19	32, 49, 44	32, 49, 44	45.56%	45.56%
63	76, 54, 49	76, 54, 90	63.33%	54.44%
66	76, 90, 54	76, 90, 54	54.44%	54.44%
79	76, 90, 54	76, 90, 54	54.44%	54.44%

TABLE IV
EVALUATION WITH AND WITHOUT DG WITH 8 MONITORING POINTS

Fault Location	Buses with Maximum ξ_d Levels		Search Field Reduction	
	Without DG	With DG	Without DG	With DG
19	32, 16, 49	16, 32, 49	53.33%	53.33%
63	76, 54, 49	76, 54, 90	70.00%	68.89%
66	76, 90, 54	76, 90, 64	68.89%	70.00%
79	76, 90, 64	76, 90, 64	70.00%	70.00%

From Table III, it is observed that the results are similar for HIFs at buses 19, 66 and 79. However, for the HIF at bus 63, the buses with maximum ξ_d levels changed. In fact, the insertion of DG resulted in more relevant transients at bus 90, making it to present ξ_d levels greater than those at bus 49. Even so, the search field reductions for all cases were satisfactory, being of 45.56% in the worst case when six monitored points were used. Also from Table IV, it is noted that the search field reduction increased for eight monitoring devices, achieving the order of 70%. In fact, as the number of buses per monitored area decreases, the algorithm performance is improved. Again, the DG changed the ξ_d levels at the monitored points, but it did not lead the algorithm to misoperate, attesting its reliability even in DNs with DG.

D. HIFs at Different Locations

To evaluate the proposed algorithm performance for HIFs at different locations, HIFs at buses 13, 19, 39 and 47 were simulated, considering the scenario 1 described in Table I. Fig. 12 depicts the maximum ξ_d levels at the monitored points for each case. As the low-frequency components did not present considerable variations, ξ_c waveforms are not illustrated.

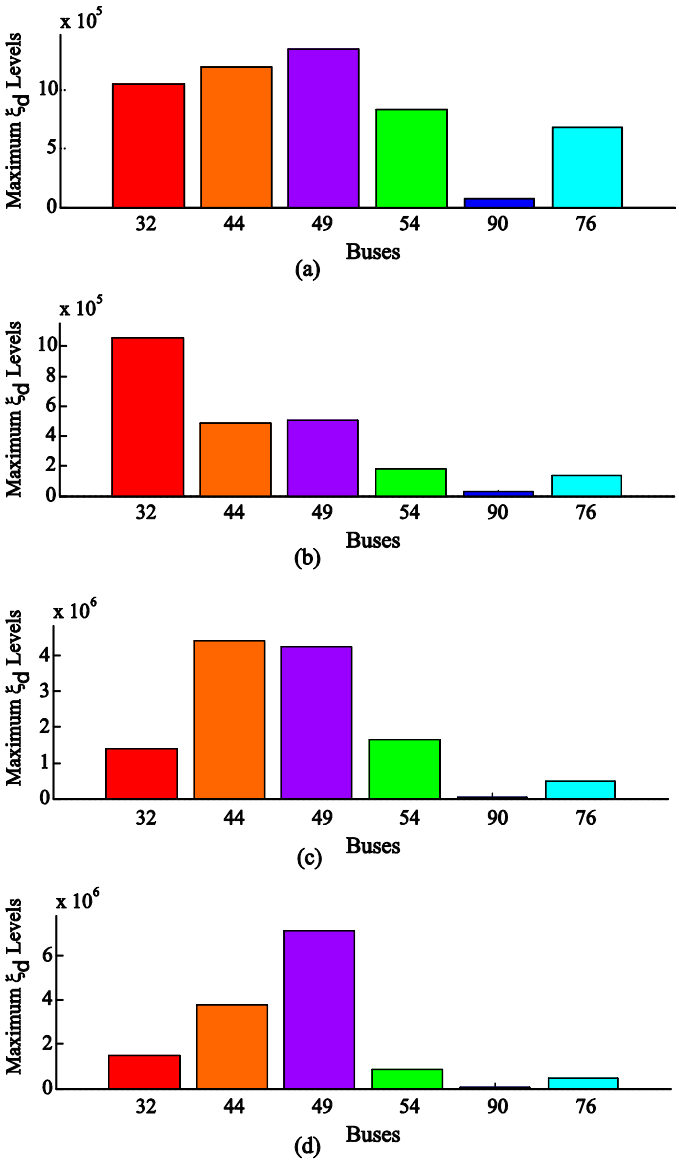

Fig. 12. Maximum ξ_d for HIF at: (a) bus 13; (b) bus 19; (c) bus 39; (d) bus 47.

In all evaluated cases, the HIF was properly detected. Also, the maximum transient energy at the monitored points varied, as expected, in accordance with the disturbance closeness to the monitoring devices.

For the HIFs at buses 13 and 19, the three maximum values of ξ_d were verified at buses 32, 44 and 49, so that the proposed algorithm indicates the HIF as being probably located in the DN areas from bus 1 to 37, from bus 38 to 44 or from bus 45 to 64. Such a conclusion results in a search field reduction of about 45.56%.

For the HIF at buses 39 and 47, the maximum values of ξ_d were detected at buses 44, 49 and 56, identifying the HIF as being probably located in the feeders from bus 45 to 49, from bus 38 to 44 or from bus 50 to 64. As a result, by taking into account the proposed algorithm outputs, maintenance crews would inspect 27 buses instead of the 90 buses of the DN, i.e., a HIF search field reduction of about 70%.

It should be pointed out that no time stamp analysis was required to obtain the reported results, revealing that the

proposed algorithm does not require data synchronization. Besides, the algorithm is simple, requires a small computational burden and does not need information regarding the feeder parameters and loads, so that it may give support, with good reliability and generality, for both off-line and online HIF diagnosis procedures in DNs.

E. Proposed Algorithm Performance during Solid Fault, Feeder Energization and Capacitor Bank Switching

In order to test the selectivity of the proposed HIF identification method, solid faults, energization of feeder branches and capacitor bank switching cases were simulated.

Fig. 13 illustrates the obtained results for solid fault cases at buses 10 and 80. In both cases, fast-risings in ξ_d were verified and relevant sags in ξ_c were detected. As a consequence, according to the flowchart shown in Fig. 5, even with the detection of transients at the monitored points, the low-frequency component analysis indicates that the disturbance is not a HIF. It should be noted that, even if the protection system fails and ξ_d remains above the threshold ρ_d for more than 150 ms, the solid fault would not be confused with a HIF, guaranteeing the proposed algorithm selectivity.

Fig. 14 shows the energies ξ_d for the energization case of the branches connected by switches in between buses 10-11 and 30-31. In these simulations, fast-risings in the energies ξ_d waveforms are observed, thereby transients are detected. Also, for both cases, the approximation coefficient energies ξ_c did not present relevant variations. However, the time period during which the energy ξ_d remained above the adaptive threshold ρ_d was smaller than 150 ms, indicating that the detected transients were not induced by a HIF. Furthermore, the transient energies were higher for buses close to the switches in-between buses 10-11 and 30-31, what can be used by the operation crews to evaluate and monitor the switching procedures in the DN.

Finally, Fig. 15 shows the obtained results for the switching cases of 0.9 Mvar and 1.8 Mvar capacitor banks at the substation. For these cases, fast-rising in the energy ξ_d waveform are observed and no relevant variations in the approximation coefficient energies ξ_c occur. As in the energization test case, for both capacitor bank switching cases, the time period during which the energy ξ_d remained above the adaptive threshold ρ_d was of about 30 ms only, not reaching the period of 150 ms expected for HIF cases and, thus, attesting that the proposed algorithm is selective.

F. Simultaneous HIFs and Solid Faults

To evaluate the influence of simultaneous HIFs and solid faults on the proposed HIF identification algorithm, four different test cases were simulated: simultaneous HIFs at the same phase; simultaneous HIFs at different phases; simultaneous HIF and solid fault at the same phase; and simultaneous HIF and solid fault at different phases. In all cases, the faults were applied at buses 13 and 80. Figs. 16 and 17 show the obtained results.

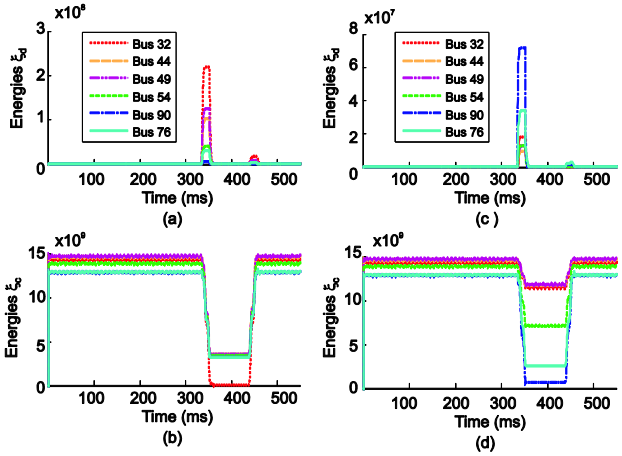

Fig. 13. Solid fault cases: (a) ξ_d for solid fault at bus 10; (b) ξ_c for solid fault at bus 10; (c) ξ_d for solid fault at bus 80; (d) ξ_c for solid fault at bus 80.

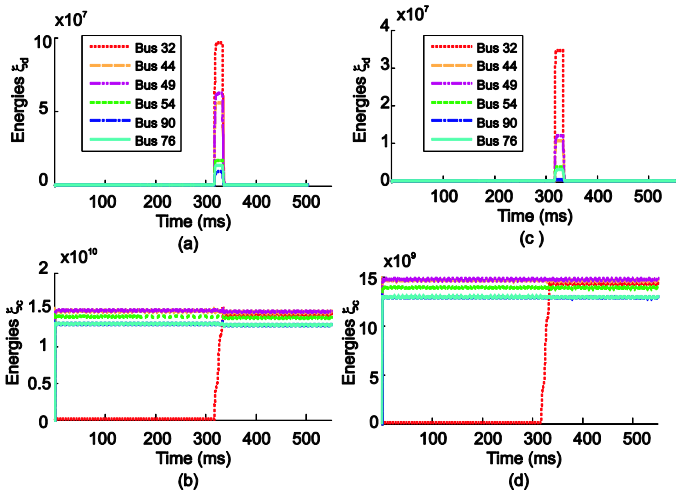

Fig. 14. Feeder energization cases: (a) ξ_d for energization at buses 10-11; (b) ξ_c for energization at buses 10-11; (c) ξ_d for energization at buses 30-31; (d) ξ_c for energization at buses 30-31.

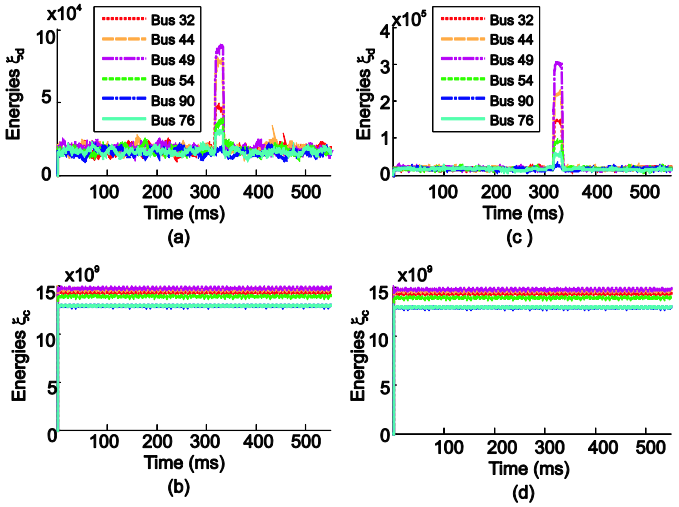

Fig. 15. Capacitor bank switching cases: (a) ξ_d for capacitor of 0.9 Mvar; (b) ξ_c for capacitor of 0.9 Mvar; (c) ξ_d for capacitor of 1.8 Mvar; (d) ξ_c for capacitor of 1.8 Mvar.

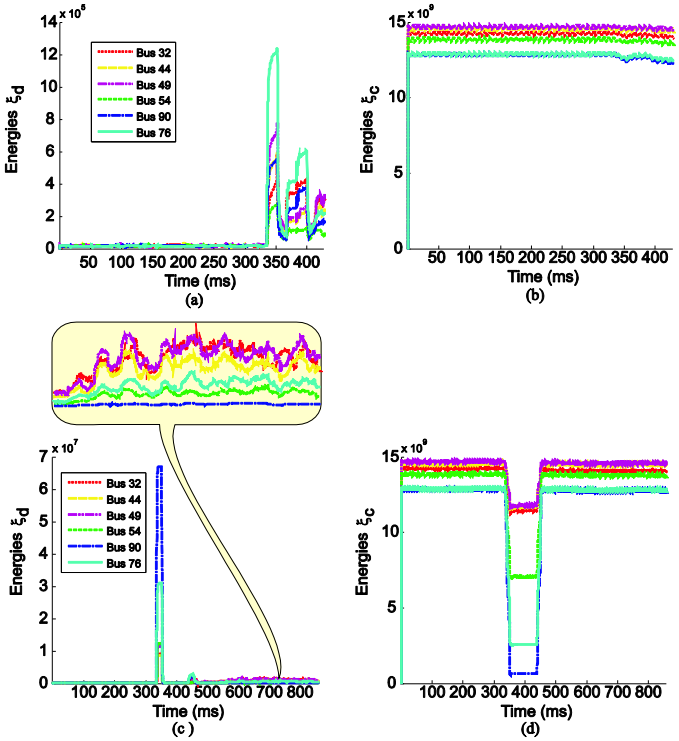

Fig. 16. Simultaneous fault cases at the same phase: (a) ξ_d for HIF at bus 13 + HIF at bus 80; (b) ξ_c for HIF at bus 13 + HIF at bus 80; (c) ξ_d for HIF at bus 13 + solid fault at bus 80; (d) ξ_c for HIF at bus 13 + solid fault at bus 80.

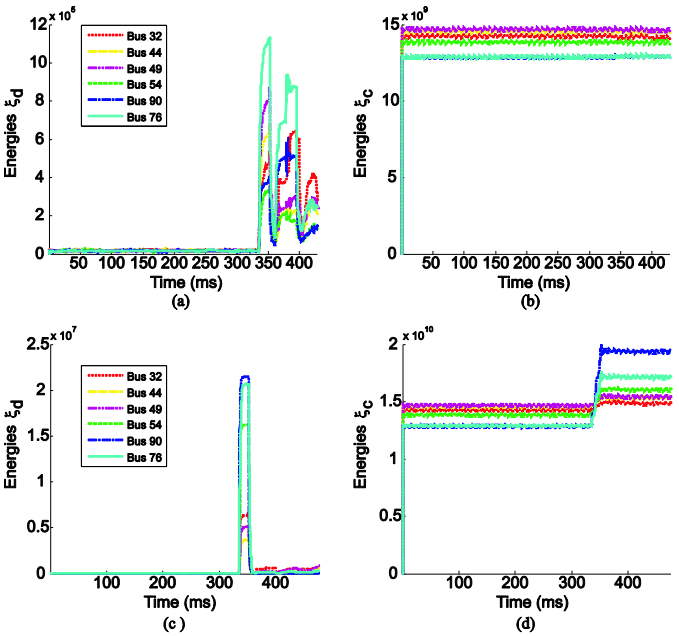

Fig. 17. Phase A quantities for simultaneous fault cases at different phases: (a) ξ_d for HIF at bus 13 phase A + HIF at bus 80 phase C; (b) ξ_c for HIF at bus 13 phase A + HIF at bus 80 phase C; (c) ξ_d for HIF at bus 13 phase A + solid fault at bus 80 phase C; (d) ξ_c for HIF at bus 13 phase A + solid fault at bus 80 phase C.

In all simulations, the most relevant ξ_d levels were detected at the buses closer to the disturbances. However, in these cases, the HIF search field reduction was compromised, since the algorithm indicates that the fault is probably in areas far from each other, in such a way that maintenance crews would have to inspect almost the whole feeder. Even so, the monitored areas with the major ξ_d values are still a good indicator of the location of HIFs along the DN, in such a way that, even with simultaneous faults, the proposed algorithm can give support to the post-fault analysis.

It was verified that transients show up in healthy conductors' measurements due to the mutual coupling between phases. However, ξ_d in faulted phases is higher than those in healthy phases, what allows the phase selection if it is desired. Besides, it was verified that ξ_d is higher than ρ_d over an interval shorter than 150 ms, even for simultaneous solid faults, so that the proposed algorithm could distinguish HIFs from solid faults. Moreover, in relation to solid faults, sags are observed at the faulted conductor measurements, whereas swells are seen in the healthy conductor measurements.

According to information given by utilities, simultaneous faults and HIFs are rare, but not impossible. Therefore, even not providing a significant search field reduction of the HIF in simultaneous fault cases, the algorithm is still useful, as it is able to detect the HIF, requiring neither data synchronization nor feeder and load parameter information.

VI. Conclusions

In this paper, a transient-based algorithm for HIF identification on distribution networks was presented. The technique analyzes the HIF-induced high- and low-frequency voltage components in order to detect the disturbance, distinguishing it from other events (such as solid faults and switching maneuvers) and identifying the area within which the HIF probably has occurred. To do so, the energy spectrum of the detail and approximation coefficients obtained using the discrete wavelet transform are computed and analyzed.

Although the method can be applied off-line, it is suitable for real-time applications, since it is simple, it does not require information regarding the feeder parameters and loads, and it does not need the time synchronization of monitoring devices. As a consequence, the proposed algorithm demonstrates to be suitable for any distribution network, provided that there are several monitoring points throughout the system.

The obtained results showed the proposed HIF identification algorithm is efficient and reliable. In the analyzed cases, the HIFs were properly identified and search field reductions in the order of 70% were achieved.

VII. Acknowledgments

The authors thank the *Coordenação de Aperfeiçoamento de Pessoal de Nível Superior* (CAPES) [Brazilian Coordination for Improvement of Higher Education Personnel] for the financial support and the editor/reviewers for the suggestions.

VIII. References

[1] J. Tengdin, R. Westfall, and K. Stephan, "High impedance fault detection technology," Rep. PSRC Working Group D, 1996, vol. 15.

[2] W. Santos, B. Souza, N. D. Brito, F. Costa, M. Paes Jr, "High Impedance Faults: From Field Tests to Modeling", in *Journal of Control, Automation and Electrical Systems*, vol 24, no 6, Sep 2013.

[3] Abradee - Brazilian Association of Electricity Utilities, *IX National Week of Population Safety with Electricity*, Brazil, 2015.

[4] J. Izykowski, R. Molag, E. Rosolowski, and M. Saha, "Accurate location of faults on power transmission lines with use of two-end unsynchronized measurements," in *IEEE Transactions on Power Delivery*, vol. 21, no. 2, pp. 627 – 633, April 2006.

[5] F. B. Costa, "Fault-Induced Transient Detection Based on Real-Time Analysis of the Wavelet Coefficient Energy", in *IEEE Transactions on Power Delivery*, vol. 29, no. 1, February 2014.
[6] F. V. Lopes, D. Fernandes Jr., and W. Neves, "Real-Time Traveling-Wave-Based Fault Location Using Two-Terminal Unsynchronized Data" , in *IEEE Trans. on Power Del.*, vol. 30, no. 3, June 2015.
[7] F. Costa, B. Souza, N. Brito, J. A. C. B. Silva, and W. C. Santos "Real-Time Detection of Transients Induced by High Impedance Faults Based on the Boundary Wavelet Transform", in *Industry Applications, IEEE Transactions on*, May 2015, vol. PP, issue:99.
[8] B. M. Aucoin, B. D. Russell, "Distribution High Impedance Fault Detection Utilizing High Frequency Current Components," in *IEEE Transactions on Power Apparatus and Systems*, vol.PAS-101, no.6, pp.1596-1606, June 1982. doi: 10.1109/TPAS.1982.317209.
[9] C. L. Benner, B. D. Russell, "Practical high-impedance fault detection on distribution feeders," in *IEEE Transactions on Industry Applications*, vol.33, no.3, pp.635-640, May/Jun 1997. doi: 10.1109/28.585852.
[10] C. J. Kim, B. D. Russell, "High-impedance fault detection system using an adaptive element model," in *IEE Proceedings Generation, Transmission and Distribution*, vol.140, no.2, pp.153-159, Mar 1993.
[11] J. Stoupis, M. Maharsi, R. Nuqui, S. A. Kunsman, and R. Das, "Ground alert: reliable detection of high-impedance faults caused by downed conductors," *ABB Review*, no. 1, pp. 28–32, 2004.
[12] J. M. Peterson, S. A. Kunsman, M. Maharsi and J. Stoupis, "Digital Signal Processor Implementation of High Impedance Fault Algorithms," U. S. Patent 0231862. [S.l.], Oct, 2005.
[13] Z. Wang, V. Donde, F. Yang, J. Stoupis, "A Deterministic Analysis Method for Back-feed Power Restoration of Distribution Networks", *Power & Energy Society General Meeting*, PES '09. IEEE. 2009.
[14] J. T. A. Vianna ; L. R. Araujo ; D. R. R. Penido, "High Impedance Fault Area Location in Distribution Systems Based on Current Zero Sequence Component", *IEEE Latin America Transactions*, Volume:14 , Issue: 2, 2016.
[15] M. M. Saha, J. Izykowski, and E. Rosolowski, *Fault Location on Power Networks*, ser. Power Systems. London: Ed. Springer, 2010.
[16] A. N. Milioudis, G. T. Andreou, and D. P. Labridis, "Enhanced Protection Scheme for Smart Grids Using Power Line Communications Techniques—Part I: Detection of High Impedance Fault Occurrence", in *IEEE Transactions on Smart Grid*, vol. 3, no. 4, December 2012.
[17] M. Michalik, W. Rebizant, M. Lukowicz, S.-J. Lee, and S.-H. Kang, "High-Impedance Fault Detection in Distribution Networks With Use of Wavelet-Based Algorithm", in *IEEE Transactions on Power Delivery*, vol. 21, no. 4, October 2006.
[18] F. V. Lopes, W. C. Santos, D. Fernandes Jr., W. L. A. Neves, and B. A. Souza, "An adaptive fault location method for smart distribution and transmission grids," in *Innovative Smart Grid Technologies (ISGT Latin America), 2011 IEEE PES Conference on*, oct. 2011, pp. 1 –7.
[19] M. Yang., J. Guan, and J. Gu, "High Impedance Faults Detection Technique Based on Wavelet Transform", in *International Journal of Electrical, Computer and Systems Engineering*, vol.1, n.3, 2007.
[20] N. Elkalashy, M. Lehtonen, H. Darwish, A.-M. Taalab, and M. Izzularab, "DWT-based detection and transient power direction-based location of high-impedance faults due to leaning trees in unearthed mv networks," in I*EEE Trans. Power Del.*, vol. 23, no. 1, pp. 94–101, 2008.
[21] A.H. Etemadi and M. Sanaye-Pasand, "High-impedance fault detection using multi-resolution signal decomposition and adaptive neural fuzzy inference system", in *IET Gener. Transm. Distrib.*, pp. 110–118, 2008.
[22] S. Nam, J. Park, Y. Kang, and T. Kim, "A modeling method of a high impedance fault in a distribution system using two series time-varying resistances in EMTP," in *2001 Power Engineering Society Summer Meeting*, vol. 2, 2001, pp. 1175 –1180 vol.2.
[23] EPRI, "EPRI Report: Detection of Arcing Faults on Distribution Feeders," Palo Alto, Tech. Rep., 1982.
[24] A.-R. Sedighi, M.-R. Haghifam, O. Malik, and M.-H. Ghassemian, "High impedance fault detection based on wavelet transform and statistical pattern recognition," *Power Delivery, IEEE Transactions on*, vol. 20, no. 4, pp. 2414 – 2421, oct. 2005.
[25] D. B. Percival and A. T. Walden, *Wavelet Methods for Time Series Analysis*. Cambridge, U.K: Cambridge University Press, 2000.
[26] S. Santoso, E. Powers, and W. Grady, "Power quality disturbance data compression using wavelet transform methods," *IEEE Transactions on Power Delivery*, vol. 12, no. 3, pp. 1250 –1257, July 1997.
[27] ONS – Brazilian National Power System Operator, *Submodule 2.6, Minimum requirements for protection and telecommunications systems*, Brazil, 2009.
[28] ANEEL – Brazilian National Electricity Agency, *Module 3 (PRODIST), Access to distribution system*, Brazil, 2008.
[29] J. C. Das, *Transients in Electrical Systems: Analysis, Recognition and Mitigation*, 1st edition, Ed. McGraw-Hill, USA, 2010.
[30] A. S. Sedra, K.C. Smith, *Microelectronic Circuits*. 6th Ed., Oxford University Press, 2009.
[31] J. C. Whitaker, *AC Power Systems Handbook*. 2nd Ed., Boca Raton, Florida, USA, CRC Press, 1999.

IX. BIOGRAPHIES

Wellinsílvio C. Santos (STM'11) received his B.Sc. and M.Sc. degrees in Electrical Engineering from Federal University of Campina Grande (UFCG), Brazil, in 2009 and 2011, respectively. He is currently a Ph.D. student at UFCG and works as a professor at Federal University of Alagoas (UFAL). His research activities are mainly focused on electromagnetic transients, high impedance fault modeling and power quality.

Felipe V. Lopes (M'10) received his B.Sc., M.Sc., and Ph.D. degrees in Electrical Engineering from Federal University of Campina Grande (UFCG), Brazil, in 2009, 2011, and 2014, respectively. He works as a professor at the Department of Electrical Engineering at University of Brasília (UnB). His research interests are electromagnetic transients, power system protection, fault location and real-time simulations.

Núbia S. D. Brito (M'05) received her B.Sc and Ph.D. in Electrical Engineering from Federal University of Paraíba (UFPB), Brazil, in 1988 and 2001 respectively. She received her M.Sc. from Campinas State University, Brazil. She works as a professor at the Department of Electrical Engineering of Federal University of Campina Grande (UFCG), Brazil. Her main research activities are on power quality, especially on applications that involve fault detection and classification in electric systems.

Benemar A. Souza (M'02 - SM'05) received his Ph.D. in Electrical Engineering from Federal University of Paraíba (UFPB), Brazil, in 1995. He works as a professor at the Department of Electrical Engineering of Federal University of Campina Grande (UFCG), Brazil. His main research activities are on optimization methods applied to power systems, electromagnetic transients, power quality and fault diagnosis.